



Published in final edited form as:

ACS Nano. 2014 January 28; 8(1): 495–502. doi:10.1021/nn405012h.

Size-Controlled Self-assembly of Superparamagnetic Polymersomes

Robert J. Hickey¹, Jason Koski², Xin Meng³, Robert A. Riggelman², Peijun Zhang³, and So-Jung Park^{1,4,*}

¹Department of Chemistry, University of Pennsylvania, 231 S South 34th Street, Philadelphia, PA 19104

²Department of Chemical and Biomedical Engineering, University of Pennsylvania, 220 S South 33rd Street, Philadelphia, PA 19104

³Department of Structural Biology, University of Pittsburgh School of Medicine, 3501 5th Avenue, Pittsburgh, PA 15260

⁴Department of Chemistry and Nano Science, Global Top 5 Program, Ewha Womans University, 52 Ewhayeodae-gil, Seodaemun-gu, Seoul, 120-750, Korea

Abstract

We report the size-controlled self-assembly of polymersomes through the cooperative self-assembly of nanoparticles and amphiphilic polymers. Polymersomes densely packed with magnetic nanoparticles in the polymersome membrane (magneto-polymersome) were fabricated with a series of different sized iron oxide nanoparticles. The distribution of nanoparticles in a polymersome membrane was size-dependent; while small nanoparticles were dispersed in a polymer bilayer, large particles formed well-ordered superstructure at the interface between the inner and outer layer of a bilayer membrane. The yield of magneto-polymersomes increased with increasing the diameter of incorporated nanoparticles. Moreover, the size of polymersomes was effectively controlled by varying the size of incorporated nanoparticles. This size-dependent self-assembly was attributed to the polymer chain entropy effect and the size-dependent localization of nanoparticles in polymersome bilayers. The transverse relaxation rates (T_2) of magneto-polymersomes increased with increasing the nanoparticle diameter and decreasing the size of polymersomes, reaching $555 \pm 24 \text{ s}^{-1}\text{mM}^{-1}$ for $241 \pm 16 \text{ nm}$ polymersomes, which is the highest value reported to date for superparamagnetic iron oxide nanoparticles.

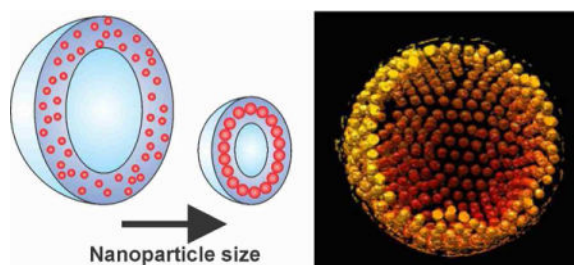
TOC image

*Corresponding author: sojungpark@ewha.ac.kr.

Supporting Information. Additional characterization data, plots of inverse transverse relaxation time ($1/T_2$) versus iron molar concentration, and a detailed description of SCFT calculations. This material is available free of charge via the Internet at <http://pubs.acs.org>.

Notes

The authors declare no competing financial interests.



Keywords

Block copolymer; nanoparticle; polymersome; vesicle; amphiphilic; superparamagnetic

Vesicles made of amphiphilic polymers (polymersomes) have received significant attention in recent years for a number of applications such as *in vivo* imaging and drug delivery due to their structure and properties mimicking biological membranes^{1–3} as well as their chemical versatility.^{4–7} For successful implementation of polymersomes in many of the applications, it is critical to fabricate size-controlled polymersomes loaded with desired functional encapsulates.^{2, 8, 9} In nature, biological vesicles can adopt a broad range of membrane curvatures and sizes through the intricate and dynamic interactions between phospholipid bilayers and nanometer-scale cellular components (*e.g.*, membrane proteins),¹⁰ which is important in many biological processes.¹¹ Here, we show that a similar structural behavior occurs in the binary self-assembly of amphiphilic polymers and artificial nanoparticles, and demonstrate that size-controlled polymersomes can be formed by the incorporation of nanoparticles in the polymersome membrane.

It is indeed a challenging task to prepare uniform sized polymersomes with a desirable diameter. Commonly used fabrication techniques typically produce polydisperse assemblies with broad size distributions^{12, 13} because vesicle formation depends much on nonequilibrium aspects of the assembly process.¹⁴ For example, polymersomes formed by the film hydration method possess a size distribution ranging from ~ 100 nm to ~ 10 μ m. Therefore, post-assembly processes such as membrane extrusion, sonication, freeze-thaw cycles are typically used to narrow the size distribution.^{15–18} Recently, a few elegant approaches have been developed to fabricate uniform sized polymer vesicles.^{19, 20} For example, Ryan *et al.* reported that micrometer-sized polymersomes with low polydispersity can be fabricated by the hydration of lithographically patterned block-copolymer films.¹⁹ Weitz and coworkers showed that highly monodisperse polymersomes can be fabricated using a microfluidic device.²⁰ For smaller submicrometer-sized polymersomes, which are much needed for *in vivo* applications,⁹ inkjet,²¹ microfluidics,²² and nanoprecipitation^{23–25} methods have been successively utilized to make polymersomes with narrow size distribution.

Herein, we report a novel approach to fabricate size-controlled sub-micrometer polymersomes based on the cooperative self-assembly of inorganic nanoparticles and amphiphilic polymers and show how the size of nanoparticles influences the binary self-assembly. We show that the incorporated nanoparticles in polymersome membranes control

the membrane curvature and the size of polymersomes through the size-dependent localization of nanoparticles in the polymersome membrane. Based on the approach, we fabricated uniform submicrometer sized superparamagnetic polymersomes loaded with iron oxide nanoparticles (magneto-polymersomes) in controllable diameters, and achieved exceptionally high transverse relaxation rates.²⁶

RESULTS AND DISCUSSION

In typical experiments, magneto-polymersomes were formed by inducing the self-assembly of amphiphilic polymers in the presence of oleic acid-stabilized iron oxide nanoparticles by the slow water addition method, following our previously reported procedure (Figure 1a).²⁷ A series of different sized iron oxide nanoparticles (5.6 ± 0.5 nm, 5.8 ± 0.7 nm, 6.4 ± 0.5 nm, 9.9 ± 0.8 nm, 10.8 ± 0.7 nm, 15.5 ± 0.8 nm, 16.3 ± 1.1 nm, and 19.9 ± 1.3) were synthesized by a modified literature procedure^{28, 29} to study the nanoparticle size effect on the self-assembly of magneto-polymersomes. The as-synthesized nanoparticles were assembled with an amphiphilic polymer of poly(acrylic acid) and polystyrene (PAA-*b*-PS) without any surface modification (Figure 1a).²⁷ Briefly, PAA₃₈-*b*-PS₇₃ in 1,4 dioxane (dioxane, 1500 μ L) and nanoparticles in tetrahydrofuran (THF, 50 μ L) were first mixed together at 25 nanoparticle weight percent (np wt%). Then, 600 μ L of water was slowly added to the solution at the rate of 10 μ L/30 sec for 30 min to induce self-assembly of amphiphilic polymers and nanoparticles. Resulting co-assemblies were dispersed in water by dialysis and centrifugation and characterized by dynamic light scattering (DLS) and transmission electron microscopy (TEM).

The TEM images showed well-defined polymersomes densely loaded with nanoparticles in the polymersome membrane (Figure 1). Cryo-TEM images (Figure 1c–d and f–g) revealed that the broken polymersomes shown in normal TEM images (Figure 1e) are actually intact when dispersed in water (Figure 1f–g). They also show that large nanoparticles (19.9 nm, Figure 1f–g) form well-ordered curved two-dimensional superlattices^{30, 31} in the polymersome membrane (*vide infra*).

To confirm the hollow structure of polymersomes, magneto-polymersomes assembled with 10.8 nm and 16.3 nm particles were imaged by TEM tomography (Figure 2, Movie 1, and Movie 2). At roughly the half-way slicing through the vesicle containing 10.8 nm particles (Figure 2a.v, Movie 1), clear polymer edges are seen on both sides of nanoparticles. The three-dimensional (3-D) surface rendering of the tomographic volume (Figure 2b) also confirms the hollow structure with nanoparticles located in the vesicle wall. The tomography data of magneto-polymersomes containing 16.3 nm particles (Figure 2c, Movie 2) shows well-ordered arrays of nanoparticles as well as the hollow structure.

In order to investigate the nanoparticle size effect on the self-assembly of magneto-polymersomes, a range of different sized nanoparticles were self-assembled with a micelle-forming polymer with a relatively short PS, PAA₃₈-*b*-PS₇₃ at a constant nanoparticle weight percent (25 np wt%) (Figure 3). The incorporation of nanoparticles induced a micelle-to-vesicle morphology change, consistent with our previous result,²⁷ yielding mixtures of magneto-polymersomes (Figure 3a–c, blue arrows) and magneto-micelles (Figure 3a–c, red

arrows) in varying ratios. Interestingly, the population of polymersomes increased with the size of nanoparticles and reached 82% polymersome yield for 16.3 nm particles (Figure 3d), revealing that the diameter of incorporated nanoparticles is an important factor that affects the polymersome formation. We hypothesize that the size-dependent polymersome yield is due to the entropic cost of inserting large nanoparticles in a polymer domain. This factor should be especially important for amphiphilic polymers with a relatively short hydrophobic block used in this study. As mentioned above, cryo-TEM and TEM tomography data showed that large nanoparticles form ordered two-dimensional superlattices (Figure 2c, Figure 4c) presumably at the PS-PS interface between the inner and outer layer of the polymersome membrane (Figure 4d (right)). The formation of ordered superlattices is believed to be the result of the large entropic cost caused by inserting large nanoparticles within a PS domain. Small particles on the other hand can be dispersed in a polymer domain of polymersomes (Figure 4a, Figure 4d (left)) or micelles (Figure 1c) without causing too much entropic penalty. Similar behavior has been observed in thin film self-assembly studies of A-B block copolymers and A-grafted nanoparticles, where large nanoparticles were segregated to the center of A domain of a lamella phase while small particles were embedded within a polymer domain.³² Note that in solution phase self-assembly studied here, a large area A-A polymer interface is obtained by adopting vesicle or bilayer structures. Therefore, the addition of large particles can induce effective micelle-to-vesicle morphology changes.

To further understand the nanoparticle-induced morphology change, we modeled our system in two dimensions using a variation of polymer self-consistent field theory (SCFT)^{33, 34} known as the hybrid particle-field theory.³⁵ Polymer chains were treated on a coarse-grained scale as A-B diblock copolymers immersed in a solvent that is chemically identical to the hydrophilic A block of the copolymer. The interactions between the hydrophilic components (A), hydrophobic polymer block (B), and the nanoparticles were each captured through a set of distinct Flory χ parameters to ensure strong phase separation between A and B components and preferential wetting of nanoparticles by the hydrophobic B block of the copolymer. The relative free energy and polymer chain entropy were calculated under a variety of nanoparticle loading conditions for two different nanoparticle sizes and varying volume fraction of the hydrophilic polymer (f_A). Representative images of nanoparticle-loaded micelles and polymersomes used in the calculations are shown in supporting information (Figures S5 and S6). The calculated free energy and entropy values are plotted as a function of f_A in Figures 3e and 3f. In the absence of nanoparticles, micelles were found to be more stable than vesicles for a wide range of f_A ($f_A > 0.3$) (Figure 3e, black). Upon the incorporation of nanoparticles, the free energy of vesicles (F_V) became substantially lower than that of micelles (F_M) at all calculated values of f_A (Figure 3e, green and red), indicating that the vesicle structure becomes more stable than micelles with the addition of nanoparticles. The entropic penalty of forming polymersomes relative to that of forming micelles is significantly reduced with the incorporation of nanoparticles (Figure 3f), supporting that the polymer entropy indeed contributes to the nanoparticle-induced polymersome formation. While these calculations do not necessarily predict that the simulated polymersomes are the most stable structure, they clearly show how the polymersome formation can be favored over micelles in the presence of nanoparticles.

Furthermore, the stabilization of polymersomes was found to be more pronounced for larger particles (Figure 3e, f), which explains the experimentally observed size-dependent polymersome yield shown in Figure 3d. When the nanoparticle radius (R_p) was increased from $1.34 R_g$ to $2.24 R_g$, where R_g is the radius of gyration of the block copolymer, the free energy difference between the polymersomes and micelles became significantly larger (Figure 3e, green and red). The entropic cost for incorporating nanoparticles in micelles compared to that in vesicles was also found to be substantially larger for larger particles for a wide range of f_A (Figure 3f). These results are consistent with our hypothesis that the entropic cost of incorporating nanoparticles in a polymer matrix is responsible for the micelle-to-vesicle morphology change.

Interestingly, we found that the size of polymersomes can be effectively controlled by varying the size of incorporated nanoparticles. The TEM (Figure 3g) and DLS (Figure S2) measurements revealed that the polymersome size gradually decreased with increasing the size of nanoparticles, as illustrated in Figure 3h. We attribute the size-controlled assembly of polymersomes to the asymmetric layer structure of vesicle membranes and the size-dependent nanoparticle distribution in the membrane. The bilayer making up the vesicle membrane is composed of an inner and an outer layer of amphiphilic polymers with distinct molecular packing structures; the outer layer has a smaller relative volume for the hydrophobic block while the inner layer has a larger relative volume for the hydrophobic block. This distinct layer structure is shown to be important for the formation of vesicles. For example, Eisenberg and coworkers have reported that a mixture of different length PAA-*b*-PS tend to assemble into polymersomes by segregating polymers with longer PS chains (or shorter PAA chains) in the inner layer of polymersomes.^{36, 37} In the binary self-assembly of nanoparticles and amphiphilic polymers studied here, nanoparticles are expected to preferentially partition in the inner layer to support the asymmetric layer structure of polymersome membranes. As mentioned above, small particles (5.8 nm, Figure 4a) are dispersed throughout the membrane presumably with more particles concentrated in the inner layer. For large nanoparticles forming a monolayer at the PS-PS interface of the polymersome wall, a larger fraction of each nanoparticle should be immersed in the inner layer to support the asymmetric layer structure (Figure 4c, Figure S3). The selective localization of nanoparticles in the inner layer should be more pronounced for larger particles. Therefore, the curvature of the membrane becomes higher with the incorporation of larger particles, resulting in smaller polymersomes, as illustrated in Figure 4d. In a related work, Eisenberg and coworkers previously showed that the self-assembly of poly(amido amine) dendrimers and PAA-*b*-PS resulted in the incorporation of PS-coated dendrimers into vesicle wall.^{38, 39} In that work, the size of polymersomes became larger with larger dendrimers due to thicker vesicle wall. The size trend observed with a vesicle forming polymer and PS-coated dendrimers is the opposite of the size dependence observed here with a short polymer and alkyl-terminated hard nanoparticles. It indicates that the polymer entropy plays an important role in the morphology change and the unusual size dependence observed here with a micelle-forming polymer with short PS. On the other hand, the nanoparticle weight percent did not significantly affect the size of polymersomes (Figure 5), supporting that the change in the polymersome size with the dimension of incorporated nanoparticles is not due to the simple hydrophobic volume effect.

To evaluate the magneto-polymerosomes for their potential use as an MRI contrast agent, transverse relaxivity rates (r_2) were measured for magneto-polymerosomes prepared from different sized nanoparticles and are plotted in Figure 6 along with the size of polymerosomes. The r_2 of water surrounding nanoparticle assemblies is known to increase with increasing the nanoparticle size⁴⁰ or increasing the size of nanoparticle assemblies.^{29, 41–43} In magneto-polymerosomes studied here, the r_2 values gradually increased with increasing the nanoparticle diameter and decreasing the polymerosome size, indicating that the nanoparticle size effect is dominant.²⁶ This result is ideal as both smaller sized polymerosomes and higher r_2 values are desirable for MRI applications. Polymerosomes assembled with 15.5 nm particles had an average hydrodynamic diameter of 241 ± 16 nm (DLS), which is comparable to the size of typical polymerosomes (~ 300 nm) made by the thin film hydration and membrane extrusion.¹⁵ The r_2 value of the 241 nm magneto-polymerosomes was determined to be 555 ± 24 s⁻¹mM⁻¹, which is the highest value reported thus far for superparamagnetic iron oxide particles.²⁶

CONCLUSIONS

In summary, polymerosomes densely loaded with iron oxide nanoparticles were fabricated by the cooperative self-assembly of nanoparticles and amphiphilic polymers of PAA-*b*-PS. It was found that the yield of polymerosomes increases with the size of incorporated nanoparticles as well as nanoparticle weight fraction when a micelle-forming polymer was used for the self-assembly. The size-dependent morphology change was explained by the entropic cost caused by incorporating large nanoparticles in a polymer domain. Furthermore, we found that the size of nanoparticles determines the size of polymerosomes. This size-controlled self-assembly was explained by the partitioning of large nanoparticles towards the inner layer of polymerosome membranes, which results in a large membrane curvature. This behavior is reminiscent of how protein binding and clustering affect the curvature of cell membranes. Based on the approach, we were able to reduce the polymerosome diameter from 513 ± 76 nm to 257 ± 90 nm by increasing the nanoparticle diameter from 5.8 nm to 16.3 nm. Note that controlling the size of polymerosomes is a challenging task because typical fabrication techniques rely on kinetic processes. The nanoparticle-induced self-assembly of polymerosomes reported here provides a new and reliable way to form size-controlled hollow polymer assemblies possessing the functionalities of nanoparticles.

METHODS AND MATERIALS

Materials and instrumentation

Sodium oleate (TCI, 95%), oleic acid (Aldrich, 90%), 1-octadecene (Aldrich, 90%), 1,4-dioxane (99 +%, Extra Pure, Stabilized, Acros Organics) were used as received without further purification. THF was freshly distilled prior to use from sodium/benzophenone under nitrogen. Iron oxide nanoparticles were synthesized by a modified literature procedure.^{28, 29} Block copolymers of PAA_m-*b*-PS_n were synthesized by the reversible addition fragmentation chain transfer (RAFT) polymerization following a previously reported procedure.⁴⁴ Magnetic relaxivity measurements and iron concentrations were determined following a previously reported procedure.²⁷ Magneto-polymerosomes were characterized by

cryo-TEM following a previously reported procedure.⁴⁵ Conventional TEM images were taken using a JEOL 1400 electron microscope, cryo-TEM images were taken using both a JEOL 2010 and JEOL 2010F, and STEM images were acquired using a JEOL 2010F electron microscope. Dynamic light scattering (DLS) measurements were taken with a Malvern Zetasizer Nano Series.

Self-assembly

To generate magneto-polymersomes, iron oxide nanoparticles and PAA₃₈-*b*-PS₇₃ were self-assembled by the slow addition of water to dioxane/THF (96.8% dioxane) solution of nanoparticles and polymers. In typical experiments, a THF solution of 5.8 nm nanoparticles (50 μL of a 3.0 mg/mL) was mixed with a PAA₃₈-*b*-PS₇₃ in dioxane (500 μL , 0.9 mg/mL) at 25 wt%. Here, the weight percent of nanoparticles is defined by 100 % times the mass of nanoparticles over the combined mass of nanoparticles and polymers. The total volume of the nanoparticle/polymer solution was adjusted to 1.55 mL by adding additional dioxane. Then, water (600 μL) was slowly added (10 μL per 30 s) to the mixture of nanoparticles and block copolymers while stirring. The mixture was kept under stirring for 15 hours before adding additional water (1.5 mL) over 15 minutes. Then, the sample was dialyzed against water for 24 hours, and concentrated by centrifugation (14,000 rpm, 30 min). The purified assemblies were redispersed in 200 μL of deionized water.

TEM tomography

For electron tomography, tilted projection images collected at 1° tilt intervals from -76° to 78° were recorded with a Gatan 4K \times 4K charge-coupled device (CCD) camera (Gatan Inc., Pleasanton, CA) mounted on a Tecnai F20 electron microscope (FEI Corporation, Hillsboro, OR) equipped with a field emission gun (FEG) operating at 200 kV. An ultra-high tilt room temperature tomography holder Gatan 916 (Gatan Inc., Pleasanton, CA) was used to access high tilt angles. A series of images were recorded at a nominal magnification of 29,000 \times and at under-focus value of 1.5 μm along the tilt axis. A back-projection algorithm, as implemented in the IMOD reconstruction package,⁴⁶ was used to convert the information present in the series of tilted projection images into three-dimensional density maps. The surface rendering was generated using the Chimera software.⁴⁷

Self-consistent field theory

A two-dimensional polymer field theory was used to model nanoparticle-loaded vesicles and micelles.^{33, 34} We used a coarse-grained model of **A-B** diblock copolymers in a solvent that is chemically identical to the hydrophilic **A** block of the copolymer. As we are primarily concerned with relatively short polymers, we employed the discrete Gaussian chain model for the diblock copolymers. Each chain was consisted of 30 total segments ($N = N_A + N_B$). The composition of the diblock copolymer given as $f_A (= N_A / N)$ was varied by changing N_A while keeping N constant. Nanoparticles were introduced using the hybrid particle-field theory reported by Sides *et al.*³⁵ The repulsion between A and B components was captured by setting the Flory chi parameter of the A/B pair (χ_{AB}) to 2.0. The chi parameters of A/nanoparticle pair (χ_{AP}) and B/nanoparticle pair (χ_{BP}) were set to 0 and 5.0 respectively to enforce the preferential wetting of nanoparticles by the hydrophobic polymer block. The

detailed derivation of our model and our numerical approach is presented in the Supporting Information.

Supplementary Material

Refer to Web version on PubMed Central for supplementary material.

Acknowledgments

S.J.P. acknowledges the support from NSF career award (DMR 0847646), ARO young investigator award, and the Camille Dreyfus teacher scholar award. This work was supported in part by the National Institutes of Health (GM085043 to PZ). Cryo-TEM images were taken at the Penn Regional Nanotechnology Facility. The authors thank Dr. Doug Yates for helpful discussions on the TEM analysis. The authors thank Kevin Vargo and Eric Johnston from Professor Daniel Hammer's group for cryo-TEM training and assistance. The authors thank Professor Adrew Tsourkas and his group for their help with the relaxivity and DLS measurements. The authors thank Dr. David Vann for his help with the ICP.

References

1. Marguet M, Bonduelle C, Lecommandoux S. Multicompartmentalized Polymeric Systems: Towards Biomimetic Cellular Structure and Function. *Chem Soc Rev.* 2013; 42:512–529. [PubMed: 23073077]
2. Tanner P, Baumann P, Enea R, Onaca O, Palivan C, Meier W. Polymeric Vesicles: From Drug Carriers to Nanoreactors and Artificial Organelles. *Acc Chem Res.* 2011; 44:1039–1049. [PubMed: 21608994]
3. Kamat NP, Katz JS, Hammer DA. Engineering Polymersome Protocells. *J Phys Chem Lett.* 2011; 2:1612–1623. [PubMed: 22110844]
4. Du J, O'Reilly RK. Advances and Challenges in Smart and Functional Polymer Vesicles. *Soft Matter.* 2009; 5:3544–3561.
5. Bellomo EG, Wyrsta MD, Pakstis L, Pochan DJ, Deming TJ. Stimuli-Responsive Polypeptide Vesicles by Conformation-Specific Assembly. *Nat Mater.* 2004; 3:244–248. [PubMed: 15034560]
6. Napoli A, Valentini M, Tirelli N, Muller M, Hubbell JA. Oxidation-Responsive Polymeric Vesicles. *Nat Mater.* 2004; 3:183–189. [PubMed: 14991021]
7. Yu S, Azzam T, Rouiller I, Eisenberg A. “Breathing” Vesicles. *J Am Chem Soc.* 2009; 131:10557–10566. [PubMed: 19722630]
8. Sanson C, Diou O, Thévenot J, Ibarboure E, Soum A, Brûlet A, Miraux S, Thiaudière E, Tan S, Brisson A, et al. Doxorubicin Loaded Magnetic Polymersomes: Theranostic Nanocarriers for MR Imaging and Magneto-Chemotherapy. *ACS Nano.* 2011; 5:1122–1140. [PubMed: 21218795]
9. De Oliveira H, Thevenot J, Lecommandoux S. Smart Polymersomes for Therapy and Diagnosis: Fast Progress Toward Multifunctional Biomimetic Nanomedicines. *Wiley Interdiscip Rev: Nanomed Nanobiotechnol.* 2012; 4:525–546. [PubMed: 22761061]
10. Lipowsky, R., S. E. Structure and Dynamics of Membranes - From Cells to Vesicles. Elsevier Science; Amsterdam: 1995.
11. Baumgart T, Capraro BR, Zhu C, Das SL. Thermodynamics and Mechanics of Membrane Curvature Generation and Sensing by Proteins and Lipids. *Annu Rev Phys Chem.* 2011; 62:483–506. [PubMed: 21219150]
12. Holowka EP, Pochan DJ, Deming TJ. Charged Polypeptide Vesicles with Controllable Diameter. *J Am Chem Soc.* 2005; 127:12423–12428. [PubMed: 16131225]
13. Hayward RC, Pochan DJ. Tailored Assemblies of Block Copolymers in Solution: It Is All about the Process. *Macromolecules.* 2010; 43:3577–3584.
14. Discher DE, Eisenberg A. Polymer Vesicles. *Science.* 2002; 297:967–973. [PubMed: 12169723]
15. Ghoroghchian PP, Frail PR, Susumu K, Blessington D, Brannan AK, Bates FS, Chance B, Hammer DA, Therien MJ. Near-Infrared-Emissive Polymersomes: Self-Assembled Soft Matter for in vivo Optical Imaging. *Proc Natl Acad Sci USA.* 2005; 102:2922–2927. [PubMed: 15708979]

16. Lee JCM, Bermudez H, Discher BM, Sheehan MA, Won Y-Y, Bates FS, Discher DE. Stability and in vitro Performance of Vesicles Made With Diblock Copolymers. *Biotechnol Bioeng.* 2001; 73:135–145. [PubMed: 11255161]
17. LoPresti C, Lomas H, Massignani M, Smart T, Battaglia G. Polymersomes: Nature Inspired Nanometer Sized Compartments. *J Mater Chem.* 2009; 19:3576–3590.
18. Stoenescu R, Meier W. Vesicles with Asymmetric Membranes from Amphiphilic ABC Triblock Copolymers. *Chem Commun.* 2002:3016–3017.
19. Howse JR, Jones RAL, Battaglia G, Ducker RE, Leggett GJ, Ryan AJ. Templated Formation of Giant Polymer Vesicles with Controlled Size Distributions. *Nat Mater.* 2009; 8:507–511. [PubMed: 19448615]
20. Lorenceau E, Utada AS, Link DR, Cristobal G, Joanicot M, Weitz DA. Generation of Polymerosomes from Double-Emulsions. *Langmuir.* 2005; 21:9183–9186. [PubMed: 16171349]
21. Hauschild S, Lipprandt U, Rumpelcker A, Borchert U, Rank A, Schubert R, Förster S. Direct Preparation Loading of Lipid Polymer Vesicles Using Inkjets. *Small.* 2005; 1:1177–1180. [PubMed: 17193413]
22. Brown L, McArthur SL, Wright PC, Lewis A, Battaglia G. Polymersome Production on a Microfluidic Platform using pH Sensitive Block Copolymers. *Lab Chip.* 2010; 10:1922–1928. [PubMed: 20480087]
23. Sanson C, Schatz C, Le Meins JF, Soum A, Thévenot J, Garanger E, Lecommandoux S. A Simple Method to Achieve High Doxorubicin Loading in Biodegradable Polymersomes. *J Control Release.* 2010; 147:428–435. [PubMed: 20692308]
24. Sanson C, Schatz C, Le Meins JF, Bruzlet A, Soum A, Lecommandoux S. Biocompatible and Biodegradable Poly(trimethylene carbonate)-block-Poly(L-glutamic acid) Polymersomes: Size Control and Stability. *Langmuir.* 2009; 26:2751–2760.
25. Yildiz ME, Prud'homme RK, Robb I, Adamson DH. Formation Characterization of Polymersomes Made by a Solvent Injection Method. *Polym Advan Technol.* 2007; 18:427–432.
26. Arosio P, Thevenot J, Orlando T, Orsini F, Corti M, Mariani M, Bordonali L, Innocenti C, Sangregorio C, Oliveira H, et al. Hybrid Iron Oxide-Copolymer Micelles and Vesicles as Contrast Agents for MRI: Impact of the Nanostructure on the Relaxometric Properties. *J Mater Chem B.* 2013; 1:5317–5328.
27. Hickey RJ, Haynes AS, Kikkawa JM, Park S-J. Controlling the Self-Assembly Structure of Magnetic Nanoparticles and Amphiphilic Block-Copolymers: From Micelles to Vesicles. *J Am Chem Soc.* 2011; 133:1517–1525. [PubMed: 21208004]
28. Park J, An KJ, Hwang YS, Park JG, Noh HJ, Kim JY, Park JH, Hwang NM, Hyeon T. Ultra-Large-Scale Syntheses of Monodisperse Nanocrystals. *Nat Mater.* 2004; 3:891–895. [PubMed: 15568032]
29. Hickey RJ, Meng X, Zhang P, Park S-J. Low-Dimensional Nanoparticle Clustering in Polymer Micelles and Their Transverse Relaxivity Rates. *ACS Nano.* 2013; 7:5824–5833. [PubMed: 23731021]
30. Murray CB, Kagan CR, Bawendi MG. Synthesis and Characterization of Monodisperse Nanocrystals and Close-Packed Nanocrystal Assemblies. *Annu Rev Mater Sci.* 2000; 30:545–610.
31. Wang T, LaMontagne D, Lynch J, Zhuang J, Cao YC. Colloidal Superparticles from Nanoparticle Assembly. *Chem Soc Rev.* 2013; 42:2804–2823. [PubMed: 23104182]
32. Thompson RB, Ginzburg VV, Matsen MW, Balazs AC. Predicting the Mesophases of Copolymer-Nanoparticle Composites. *Science.* 2001; 292:2469–2472. [PubMed: 11431562]
33. Fredrickson, GH. *The Equilibrium Theory of Inhomogeneous Polymers.* Oxford University Press, USA; New York: 2006.
34. Matsen MW. The Standard Gaussian Model for Block Copolymer Melts. *J Phys: Condens Matter.* 2002; 14:R21–R47.
35. Sides SW, Kim BJ, Kramer EJ, Fredrickson GH. Hybrid Particle-Field Simulations of Polymer Nanocomposites. *Phys Rev Lett.* 2006; 96:250601. [PubMed: 16907292]
36. Luo L, Eisenberg A. Thermodynamic Stabilization Mechanism of Block Copolymer Vesicles. *J Am Chem Soc.* 2001; 123:1012–1013. [PubMed: 11456651]

37. Mai Y, Eisenberg A. Self-assembly of Block Copolymers. *Chem Soc Rev*. 2012; 41:5969–5985. [PubMed: 22776960]
38. Kroeger A, Li X, Eisenberg A. Dendrimer-Influenced Supramolecular Structure Formation of Block Copolymers. *Langmuir*. 2007; 23:10732–10740. [PubMed: 17824625]
39. Li X, Kroeger A, Azzam T, Eisenberg A. Dendrimer Influenced Supramolecular Structure Formation of Block Copolymers: II. Dendrimer Concentration Dependence. *Langmuir*. 2008; 24:2705–2711. [PubMed: 18237205]
40. Jun, Y-w, Huh, Y-M., Choi, J-s, Lee, J-H., Song, H-T., Kim, S., Yoon, S., Kim, K-S., Shin, J-S., Suh, J-S., et al. Nanoscale Size Effect of Magnetic Nanocrystals and Their Utilization for Cancer Diagnosis via Magnetic Resonance Imaging. *J Am Chem Soc*. 2005; 127:5732–5733. [PubMed: 15839639]
41. Pösel E, Kloust H, Tromsdorf U, Janschel M, Hahn C, Maßlo C, Weller H. Relaxivity Optimization of a PEGylated Iron-Oxide-Based Negative Magnetic Resonance Contrast Agent for T2-Weighted Spin-Echo Imaging. *ACS Nano*. 2012; 6:1619–1624. [PubMed: 22276942]
42. Lee N, Choi Y, Lee Y, Park M, Moon WK, Choi SH, Hyeon T. Water-Dispersible Ferrimagnetic Iron Oxide Nanocubes with Extremely High r₂ Relaxivity for Highly Sensitive in Vivo MRI of Tumors. *Nano Lett*. 2012; 12:3127–3131. [PubMed: 22575047]
43. Yoon T-J, Lee H, Shao H, Hilderbrand SA, Weissleder R. Multicore Assemblies Potentiate Magnetic Properties of Biomagnetic Nanoparticles. *Adv Mater*. 2011; 23:4793–4797. [PubMed: 21953810]
44. Sanchez-Gaytan BL, Cui WH, Kim YJ, Mendez-Polanco MA, Duncan TV, Fryd M, Wayland BB, Park SJ. Interfacial Assembly of Nanoparticles in Discrete Block-Copolymer Aggregates. *Angew Chem Int Ed*. 2007; 46:9235–9238.
45. Hickey RJ, Luo Q, Park S-J. Polymersomes and Multicompartment Polymersomes Formed by the Interfacial Self-assembly of Gold Nanoparticles Amphiphilic Polymers. *ACS Macro Lett*. 2013; 2:805–808.
46. Kremer JR, Mastrorarde DN, McIntosh JR. Computer Visualization of Three-Dimensional Image Data Using IMOD. *J Struc Biol*. 1996; 116:71–76.
47. Pettersen EF, Goddard TD, Huang CC, Couch GS, Greenblatt DM, Meng EC, Ferrin TE. UCSF Chimera—A Visualization System for Exploratory Research Analysis. *J Comput Chem*. 2004; 25:1605–1612. [PubMed: 15264254]

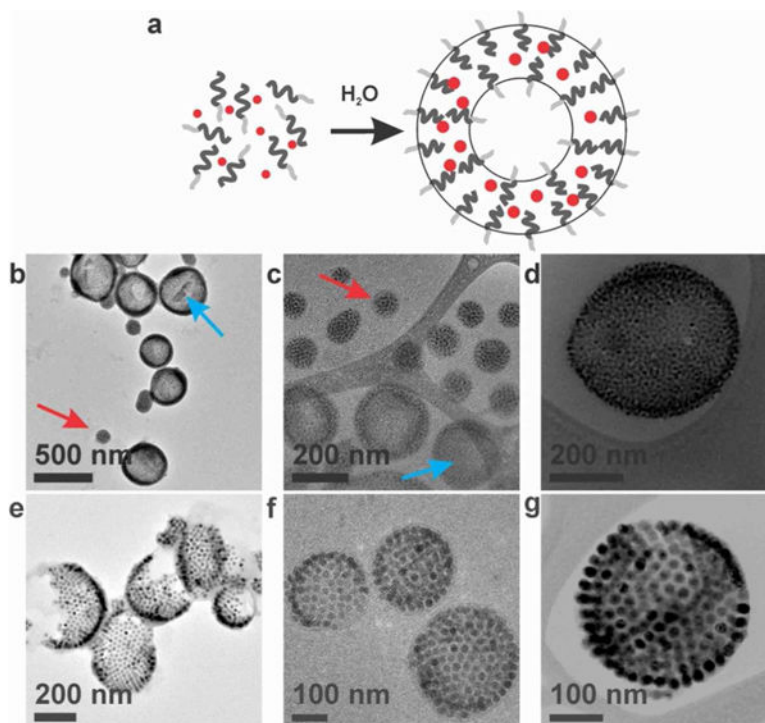


Figure 1. (a) Schematic representation of the self-assembly of magneto-polymsomes from iron oxide nanoparticles and amphiphilic block copolymers. Light gray lines, dark gray lines, and red dots represent PAA, PS, and iron oxide nanoparticles, respectively. (b–d) Conventional TEM (b) and cryo-TEM (c) and cryo-STEM (d) images of magneto-polymsomes assembled with 10.8 nm particles. Blue and red arrows indicate polymersomes and micelles, respectively. (e–g) Conventional TEM (e), cryo-TEM (f), and cryo-STEM (g) images of magneto-polymsomes assembled with 19.9 nm particles. Cryo-TEM images show intact magneto-polymsomes, indicating that the broken polymersomes observed in normal TEM (e) are due to the drying process.

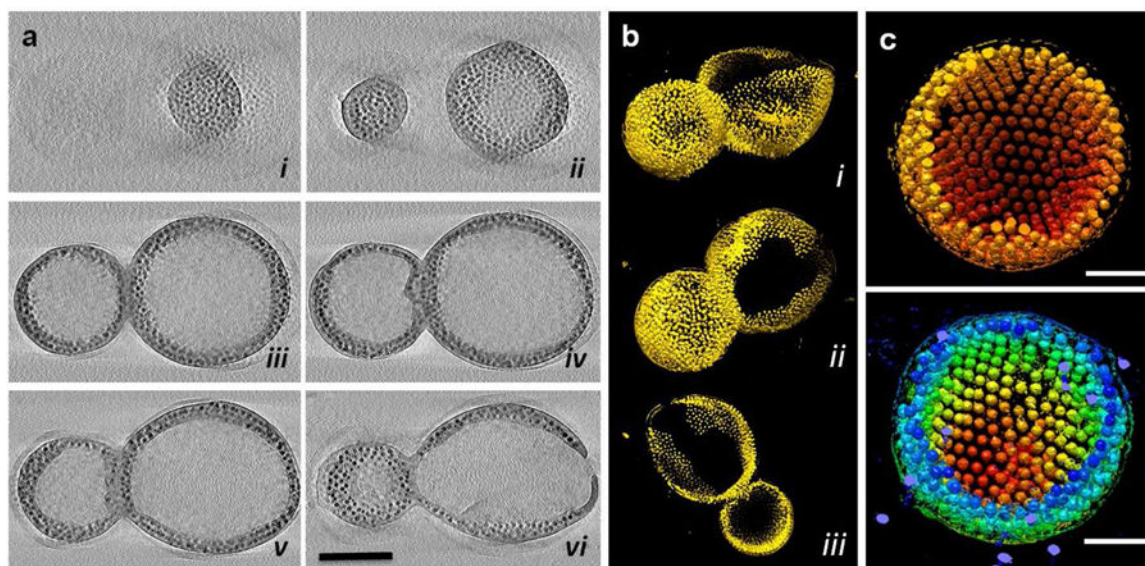


Figure 2. TEM tomography of magneto-polymsomes assembled with 10.8 and 16.3 nm iron oxide particles. (a) 0.23 nm thick X-Y computational slices (i–vi) of the 3-D tomographic volume containing magneto-polymsomes assembled with 10.8 nm iron oxide particles, shown in every 60 slices (13.8 nm) through the volume. The scale bar is for 200 nm. (b) 3-D surface rendering of the polymersomes shown in a, viewed from side (i), bottom (ii) and as a slab (iii). (c) 3-D surface rendering of a magneto-polymsome assembled with 16.3 nm iron oxide particles, showing nanoparticles form ordered arrays in the polymersome. The magneto-particles are colored red to yellow according to the radial position from the center (top) or red to blue according to the height (bottom). The scale bar is for 100 nm.

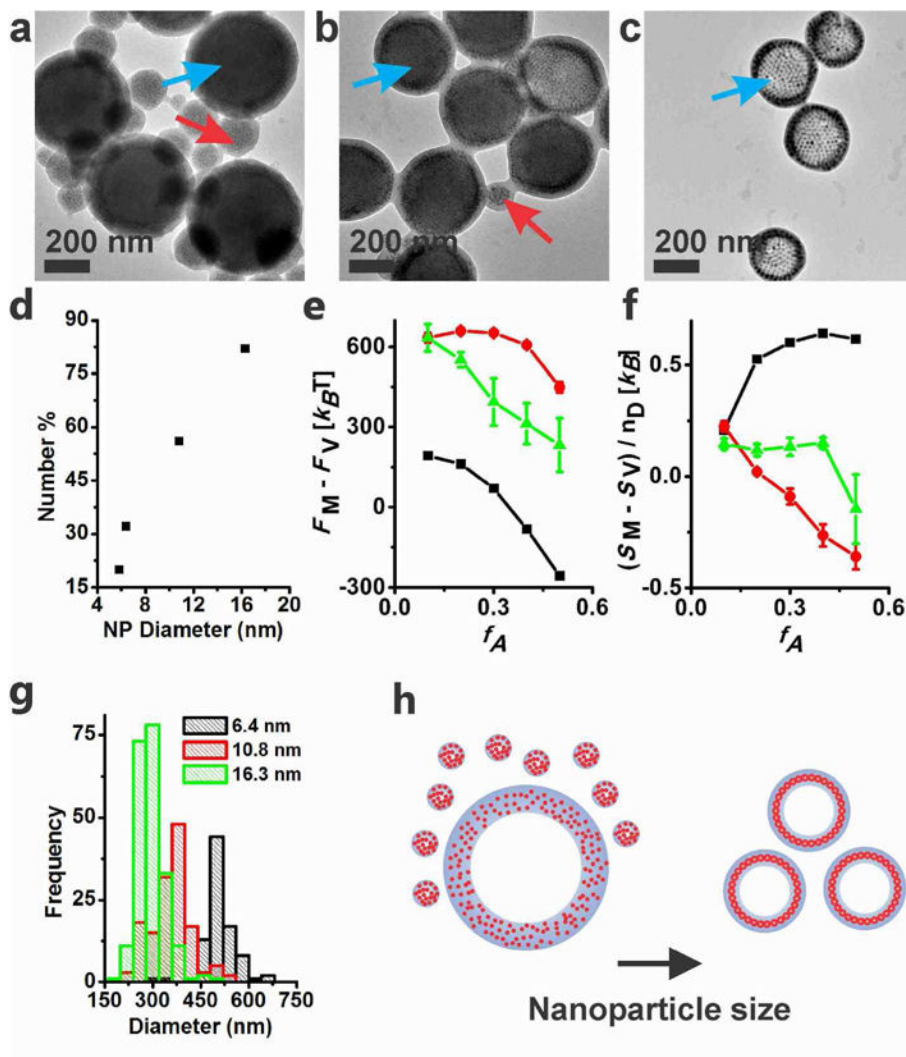


Figure 3. (a–c) TEM images of magneto-polymersomes assembled with (a) 6.4 nm, (b) 10.8 nm, and (c) 16.3 nm iron oxide particles at 25 wt %. Blue and red arrows indicate polymersomes and micelles, respectively. (d) TEM analysis of polymersome number percent, which is defined by 100% times the number of polymersomes over the number of assemblies (polymersomes and micelles). Over 200 assemblies were counted for the analysis. (e) The calculated relative Helmholtz free energy of nanoparticle-free (black) or nanoparticle-loaded (green and red) polymer assemblies as a function of f_A for two different nanoparticle radii (green: $1.34R_g$, red: $2.24R_g$). (f) The average entropy per diblock copolymer chain in vesicles (S_V) minus that in micelles (S_M). The error bars in (e) and (f) represent the standard error averaged over three different micelle configurations for the larger particle system ($2.24R_g$), and five configurations for the smaller particle system ($1.34R_g$). In all calculations, f_A was varied while keeping the chain length N of the polymer constant. (g) Size histogram of magneto-polymersomes determined by TEM. (h) A pictorial description showing how the nanoparticle size affects the polymersome population and dimension.

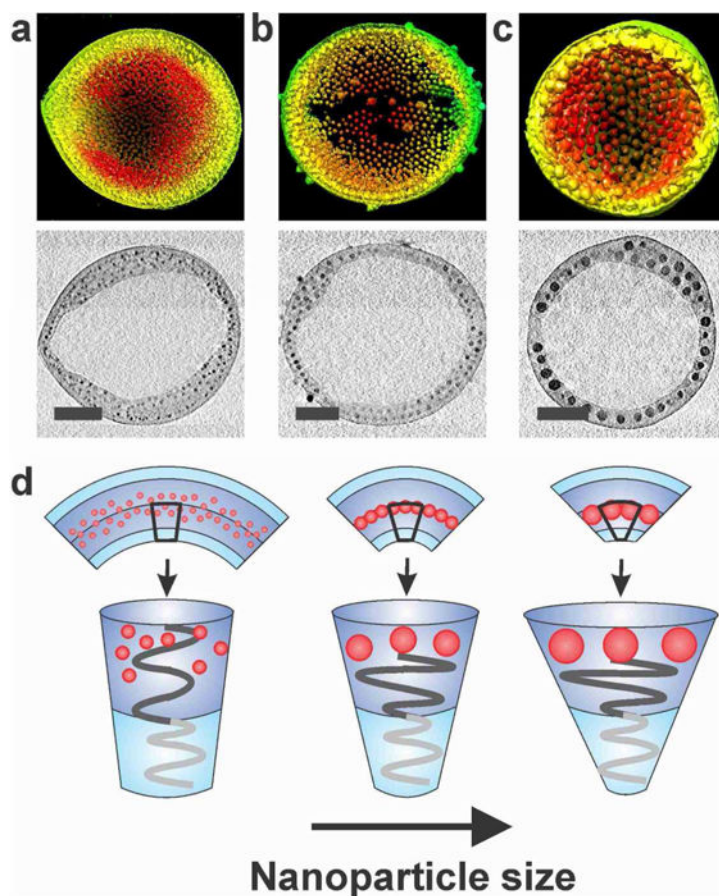


Figure 4. Reconstructed 3-D surface rendering of the tomographic volume and X-Y computational slices (0.23 nm) at the mid-point of magneto-polymersomes assembled with (a) 5.8 nm, (b) 9.9 nm, and (c) 16.3 nm iron oxide particles. Scale bars are 100 nm. (d) Pictorial representation showing how the nanoparticle size affects the curvature of polymersome membranes.

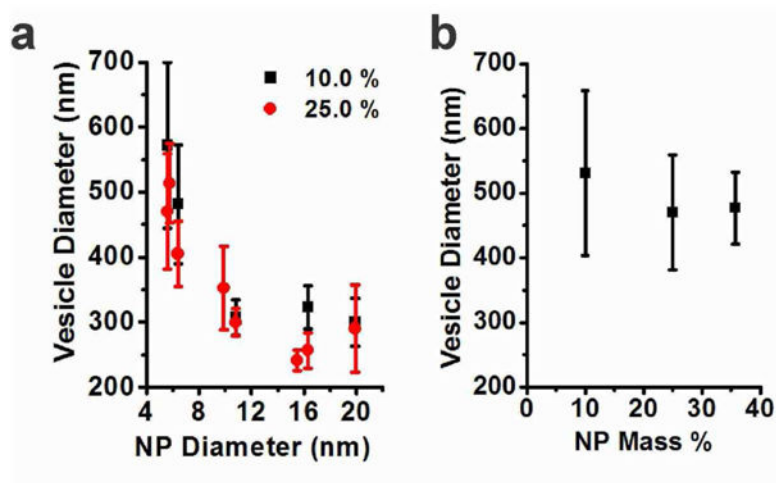


Figure 5. (a) The diameters of magneto-polymersomes incorporating 5.6, 5.8, 6.4, 9.9, 10.8, 15.5, 16.3, and 19.9 nm particles determined by DLS at two different nanoparticle weight percent. The standard deviation was calculated from three different measurements. (b) The hydrodynamic diameter of magneto-polymersomes formed with 5.6 nm particles as a function of nanoparticle weight percent.

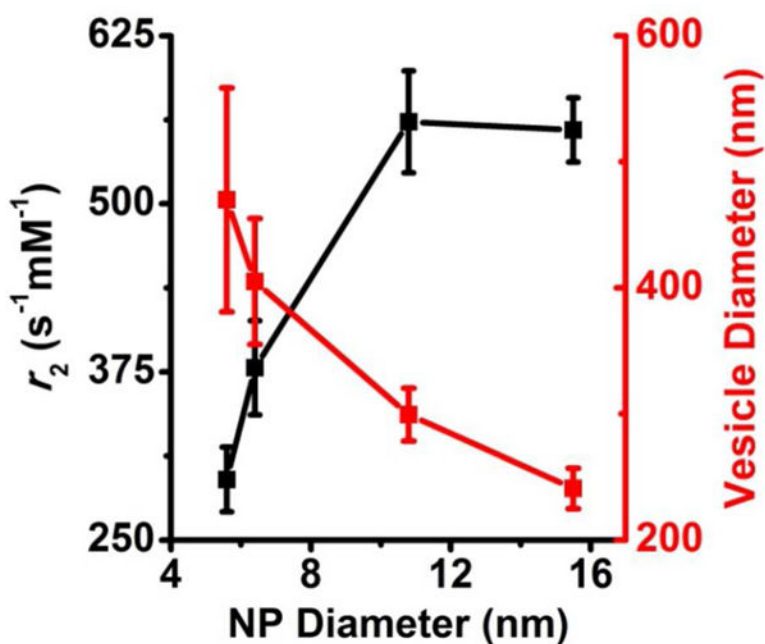


Figure 6.

Transverse relaxivity rates (r_2) for magneto-polymersomes loaded with different sized iron oxide nanoparticles at 25 np wt %. The r_2 values (black) were calculated to be $295 \pm 24 s^{-1}mM^{-1}$, $378 \pm 35 s^{-1}mM^{-1}$, $561 \pm 38 s^{-1}mM^{-1}$, and $555 \pm 24 s^{-1}mM^{-1}$ for magneto-polymersomes made from iron oxide nanoparticles of diameter 5.6 nm, 6.4 nm, 10.8 nm, and 15.5 nm, respectively. The sizes of the magneto-polymersomes (red) from Figure 5b were plotted along with the r_2 values. The standard deviations of the r_2 values were determined from at least three separate samples. The plots of inverse transverse relaxation time ($1/T_2$) versus iron molar concentration are provided in the supporting information.